AGU PUBLICATIONS

Geophysical Research Letters

RESEARCH LETTER
10.1002/2016GL068968

Special Section:
First results from NASA's Magnetospheric Multiscale (MMS) Mission

Whistler mode waves and Hall fields detected by MMS during a dayside magnetopause crossing

O. Le Contel[1], A. Retinò[1], H. Breuillard[1], L. Mirioni[1], P. Robert[1], A. Chasapis[1], B. Lavraud[2], T. Chust[1], L. Rezeau[1], F. D. Wilder[3], D. B. Graham[4], M. R. Argall[5], D. J. Gershman[6], P.-A. Lindqvist[7], Y. V. Khotyaintsev[4], G. Marklund[7], R. E. Ergun[3], K. A. Goodrich[3], J. L. Burch[8], R. B. Torbert[5], J. Needell[5], M. Chutter[5], D. Rau[5], I. Dors[5], C. T. Russell[9], W. Magnes[10], R. J. Strangeway[9], K. R. Bromund[6], H. K. Leinweber[9], F. Plaschke[10], D. Fischer[10], B. J. Anderson[11], G. Le[6], T. E. Moore[6], C. J. Pollock[6], B. L. Giles[6], J. C. Dorelli[6], L. Avanov[6], and Y. Saito[12]

[1]Laboratoire de Physique des Plasmas (LPP), UMR7648 CNRS/Ecole Polytechnique/UPMC/Université Paris-Sud/Observatoire de Paris, Palaiseau, France, [2]Institut de Recherche en Astrophysique et Planétologie (IRAP), CNRS UMR5277/Université Paul Sabatier, Toulouse, France, [3]Laboratory for Atmospheric and Space Physics, University of Colorado Boulder, Boulder, Colorado, USA, [4]Swedish Institute of Space Physics, Uppsala, Sweden, [5]University of New Hampshire, Durham, New Hampshire, USA, [6]NASA Goddard Space Flight Center, Greenbelt, Maryland, USA, [7]Royal Institute of Technology, Stockholm, Sweden, [8]Southwest Research Institute, San Antonio, Texas, USA, [9]University of California, Los Angeles, California, USA, [10]Space Research Institute, Austrian Academy of Sciences, Graz, Austria, [11]The Johns Hopkins University Applied Physics Laboratory, Laurel, Maryland, USA, [12]Institute for Space and Astronautical Science, Sagamihara, Japan

Key Points:
- A quasi-steady whistler mode wave emission is detected on the magnetospheric side, just before the opening of the magnetic field lines
- Hall electric fields are calculated and found to be consistent with the decoupling of ions from the magnetic field
- The source of the whistler mode waves is likely the perpendicular temperature anisotropy of the energetic part of the electron distribution

Correspondence to:
O. Le Contel,
olivier.lecontel@lpp.polytechnique.fr

Citation:
Le Contel, O., et al. (2016), Whistler mode waves and Hall fields detected by MMS during a dayside magnetopause crossing, *Geophys. Res. Lett.*, *43*, 5943–5952, doi:10.1002/2016GL068968.

Received 1 APR 2016
Accepted 13 MAY 2016
Accepted article online 25 MAY 2016
Published online 20 JUN 2016
Corrected 13 SEP 2016

This article was corrected on 13 SEP 2016. See the end of the full text for details.

Abstract We present Magnetospheric Multiscale (MMS) mission measurements during a full magnetopause crossing associated with an enhanced southward ion flow. A quasi-steady magnetospheric whistler mode wave emission propagating toward the reconnection region with quasi-parallel and oblique wave angles is detected just before the opening of the magnetic field lines and the detection of escaping energetic electrons. Its source is likely the perpendicular temperature anisotropy of magnetospheric energetic electrons. In this region, perpendicular and parallel currents as well as the Hall electric field are calculated and found to be consistent with the decoupling of ions from the magnetic field and the crossing of a magnetospheric separatrix region. On the magnetosheath side, Hall electric fields are found smaller as the density is larger but still consistent with the decoupling of ions. Intense quasi-parallel whistler wave emissions are detected propagating both toward and away from the reconnection region in association with a perpendicular anisotropy of the high-energy part of the magnetosheath electron population and a strong perpendicular current, which suggests that in addition to the electron diffusion region, magnetosheath separatrices could be a source region for whistler waves.

1. Introduction

The study of the interaction between the shocked solar wind and the Earth's magnetic field is a long standing problem. How, at which rate and at which scale, the energy, the mass and the magnetic flux are transferred to the magnetosphere are some of the fundamental issues. When the interplanetary magnetic field (IMF) is directed southward, magnetic reconnection is thought to be the main physical process by which these transfers happen. In such conditions, magnetic reconnection is asymmetric [*Swisdak et al.*, 2003; *Pritchett*, 2008] as it involves a cold dense plasma frozen in a large-scale magnetic field (IMF) and a hot tenuous plasma confined by magnetic mirrors; this latter property may introduce large-scale kinetic effects due to particle bounce motions [e.g., *Le Contel et al.*, 2000]. Magnetic reconnection studies taking into account asymmetric plasma density and magnetic field conditions showed important differences as compared to the symmetric case. Notably, the classical quadrupolar out-of-plane magnetic field and dipolar in-plane electric field patterns are modified to dipolar and unipolar patterns, respectively [*Mozer et al.*, 2008]. The conventional description of collisionless magnetic reconnection implies three scales: the energy is injected into the system at large magnetohydrodynamic scales (larger than the ion Larmor radius), then as thin ion scale current sheets are formed at the interface by the convecting plasma, ions decouple from the magnetic field in the so-called ion diffusion region, and finally the same decoupling happens for electrons at the smaller electron scales. The proper way to identify these regions in space measurements is still a matter of debate

[e.g., *Pritchett and Mozer*, 2009; *Scudder et al.*, 2008]. However, the comparison between the velocity of the field line motion, $\mathbf{E} \times \mathbf{B}/B^2$ and the particle motion (with strong instrumental caveats) appears to be a basic starting point. In a fluid picture, this comparison can be based on the estimation of the various terms of the generalized Ohm's law. In particular, the Hall effect related to the Lorentz force ($\mathbf{j} \times \mathbf{B}$) is considered as one of the key factors at the origin of the ion decoupling from the magnetic field [e.g., *Birn et al.*, 2001; *Wygant et al.*, 2005]. Regarding the electron dynamics, the divergence of the electron pressure tensor is also invoked for causing the violation of the electron frozen-in motion [*Pritchett and Mozer*, 2009]. Finally, in collisionless plasmas wave-particle interactions have been considered as a possible mechanism to accelerate particles, generate anomalous resistivity and locally break the frozen-in condition [see *Treumann*, 2001]. In particular, *Cattell et al.* [1995] showed that lower hybrid drift waves during an active magnetopause crossing have large enough amplitudes to provide the resistivity needed for reconnection. The instrument suite of the Magnetospheric Multiscale mission (MMS) aims to study the physics of magnetic reconnection at electron scales and in particular to identify the key factors for understanding this fundamental process [*Burch et al.*, 2015; *Torbert et al.*, 2014]. In the present paper, we present MMS measurements recorded during a complete magnetopause crossing and investigate how the whistler mode wave emissions are related to electron temperature anisotropy and Hall electric fields.

2. Observations

2.1. Overview

On 16 October 2015, the MMS tetrahedral constellation was located at [8.3, 8.5, 0.7] Earth radii (R_E) in the geocentric solar ecliptic coordinate system (GSE); the average distance between satellites was ~15 km. Figure 1 displays an overview of burst mode data from a magnetopause crossing between 1305:25 and 1306:10 UT as measured by MMS1. Figure 1a) shows fluxgate magnetometer (FGM) data at 128 samples/s (S/s) provided by the magnetic field team after a comprehensive calibration procedure [*Russell et al.*, 2014]. Data are projected into local magnetic normal coordinates (LMN). This frame of reference is obtained from a minimum variance analysis (MVA) performed around the full magnetopause crossing between 1305:40 and 1306:10 UT using MMS1 **B** data time averaged over 100 ms. The eigenvectors and eigenvalues are **L**[0.39, −0.19, 0.90], **M**[0.51, −0.77, −0.38], **N**[0.76, 0.61, −0.20] in GSE and 756, 27, and 10, respectively. The normal to the magnetopause is mainly in the GSE equatorial plane and directed about 45° toward the dusk noon sector; the direction of maximum variance is almost directed along the Z GSE axis. Note that as the results of the MVA are very similar for all spacecraft, MMS1 is chosen as reference in the rest of the study. Furthermore, though the ratio between intermediate and minimum eigenvalues is quite small, the normal direction is close to the direction obtained from the Shue's model [*Shue et al.*, 1998] and to the normal direction estimated from the maximum variance of the convective ($-\mathbf{v_i} \times \mathbf{B}$) electric field [*Sonnerup et al.*, 1987]. The BL component rotates from northward to southward. As this rotation occurs with a delay of about 120 ± 10 ms between MMS4/MMS3 and MMS1, a first rough estimate of the normal velocity is about -65 ± 10 km s^{-1} (only taking into account the time delay error and neglecting the error on the normal direction). As the density gradient region and the region of BL rotation last about 5 s, the spatial scale of the magnetopause crossing is estimated to be about 325 ± 50 km. Electron and ion energy time spectrograms, electron density (N_e), ion velocity (V_i), ion and electron temperatures (T_i, T_e) obtained from the Fast Particle Instrument (FPI) are displayed in Figures 1b–1g. The magnetopause crossing is associated with the transition between a hot tenuous energetic plasma ($N_e \sim 0.3$ cm^{-3}, $T_i \sim 2$ keV, $T_e \sim 100$ eV) and a cold dense plasma ($N_e \sim 10$ cm^{-3}, $T_i \sim 400$ eV, $T_e \sim 20$–40 eV). Note that the magnetospheric electron temperature is quite low and probably associated with a boundary layer region in the vicinity of the magnetopause. Also, the presence of energetic ions in the magnetosheath region suggests that MMS1 does not reach the unperturbed magnetosheath. A fast ion flow moving along the interface in the southward direction at velocities up to VL ~ − 300 km s^{-1} is measured while the magnetosheath flow at the end of the period corresponds to VM ~ − 130 km s^{-1}, and VL ~ − 110 km s^{-1}. For comparison, the predicted velocity jump for a rotational discontinuity using a single starting point in the magnetosheath [*Paschmann et al.*, 1986] is also plotted (dotted lines) and the ratio between measured and predicted velocities is about 0.6. Reasons for such a discrepancy are discussed by *Paschmann et al.* [1986]. From these conditions the spatial scale of the magnetopause crossing is found to be about five magnetosheath ion inertial lengths (~70 km) or three ion Larmor radii (the magnetosheath and the magnetospheric ion Larmor radii being almost equal ~150 km) whereas the outflow region lasting about 15 s (~1000 km) is 3 times larger. Both ions and electrons show periods of temperature anisotropies, in particular, the electrons undergo strong parallel heating around the crossing as discussed in the next section. Finally, Figures 1h and 1i) display

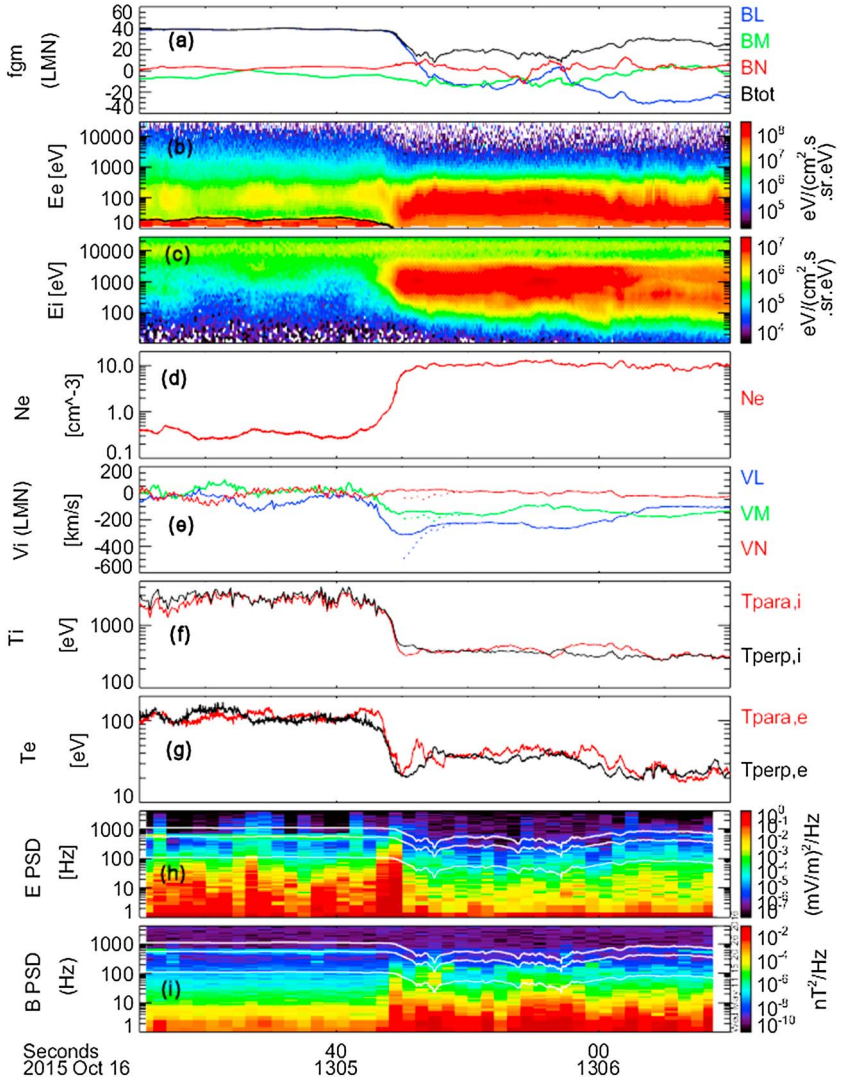

Figure 1. Overview of the magnetopause crossing by MMS1 on 16 October 2015 around 13:05:40 UT plotted in LMN coordinates: (a) **B** data at 128 samples/s, (b) electron (with superposed spacecraft potential, black line) and (c) ion omnidirectional energy time spectrograms, (d) electron density (N_e), (e) predicted (dotted line) and measured (solid lines) ion velocities (V_i), (f, g) ion and electron temperatures (T_i, T_e), (h, i) omnidirectional electric (E PSD) and magnetic (B PSD) power spectral densities. The superposed white lines correspond to 1, 0.5, and 0.1 the electron cyclotron frequency (f_{ce}).

omnidirectional electric (E PSD) and magnetic (B PSD) power spectral densities obtained from the electric and magnetic waveforms sampled at 8192 S/s by the digital signal processor [*Ergun et al.*, 2014]. They are measured by the electric double probes (EDP) [*Lindqvist et al.*, 2014; *Ergun et al.*, 2014] and the search-coil magnetometer (SCM) [*Le Contel et al.*, 2014]. From these spectra we note that a high-frequency emission is detected on the magnetospheric side just before the crossing, at frequency around 0.5 $f_{ce} \sim 600$ Hz, within the whistler mode wave frequency range. Then this emission stops and is followed by strong electrostatic and electromagnetic emissions detected just at the density gradient, and likely to be associated with the lower hybrid drift instability (LHDI) [*Cattell et al.*, 1995; *Vaivads et al.*, 2004; *Retinò et al.*, 2006]. In the magnetosheath region, intense broadband electromagnetic fluctuations up to 20 Hz are present, which have been interpreted as kinetic Alfvén waves [*Chaston et al.*, 2008; *Roux et al.*, 2011] as well as short duration emissions in the whistler mode wave frequency range, consistent with previous observations [e.g., *Deng and Matsumoto*, 2001]. Finally, this magnetopause crossing as well as the partial crossing occurring later around 1307 UT have also been investigated by *Burch et al.* [2016]. They showed that a jet reversal and a stronger electron parallel heating ($\Delta T_{\|,e} \sim 20$ eV) are measured in the second crossing in contrast with the observations of

a single southward jet and a moderate electron parallel heating ($\Delta T_{\parallel,e} \sim 20$ eV) during the first crossing. Furthermore, the decoupling of electrons from **B** and the strong dissipation observed between 1307:02.1 and 1307:02.3 UT allow them to identify the electron diffusion region probably at the origin of the southward jet detected during the first crossing if we assume a steady reconnection process at least between these two crossings. In the present paper we only analyze the first crossing and we describe the related current and electron anisotropy measurements in the next section.

2.2. Current and Electron Anisotropy

Figure 2 shows a blowup of the magnetopause crossing by MMS1 between 1305:40 and 1305:50 UT. The BL component (Figure 2a) rotates from northward to southward while BM (Figure 2b) decreases down to −12 nT on the magnetosheath side. The magnitude does not go to zero when BL changes sign as BM and BN (Figure 2c) retain significant values. The current sheet can be considered as a current sheet with a local guide field. The ion outflow region starts on the magnetospheric side while the maximum velocity occurs on the magnetosheath side (Figure 2f) where the density is about 10 cm^{-3} (Figure 2e). The ion temperature (Figure 2g) is almost isotropic except for the region of the maximum outflow velocity, where the perpendicular temperature is slightly larger than the parallel temperature. Parallel electron heating (Figure 2h) is measured both on the magnetospheric and magnetosheath sides and throughout the density gradient region. However, between 1305:47 and 1305:48 UT, the perpendicular temperature is temporarily larger than the parallel temperature. LMN currents computed from MMS1 FPI data are shown in Figure 2i and from the barycentric method [*Chanteur and Harvey*, 1998] using the four FGM measurements in Figure 2j together with the respective parallel, perpendicular, and total currents shown in Figures 2k and 2l. The agreement between the currents computed from FPI and those computed from FGM is very good taking into account that FPI corresponds to a single point measurement while FGM currents correspond to an average of the current flowing through the tetrahedral configuration. Also, FPI parallel and perpendicular currents are obtained using MMS1 FGM data, time averaged over the electron time resolution of 30 ms, while FGM parallel and perpendicular currents are obtained by a projection on a **B** field averaged over the four satellites (by the barycentric method). Both instruments measure a negative JM current of ∼−200 nA m^{-2} as BL rotates from northward to southward, which corresponds to the large-scale magnetopause current layer. Two small-scale peaks of the total current of about 500 nA m^{-2} and 400 nA m^{-2} are measured between 1305:46 and 1305:48 UT. The first peak corresponds to both large parallel and perpendicular currents, whereas the second peak is only in the perpendicular direction. Figures 2m and 2q present an electron energy time spectrogram, pitch angle distribution (pad) spectrograms for three energy ranges from low (LE PAD, [0–200 eV]), medium (ME PAD, [200eV–2keV]) to high (HE PAD, [2 keV–30 keV]) energies and finally an ion energy time spectrogram. From 1305:40.0 to 1305:43.5 UT, in the magnetosphere, HE electron fluxes are larger around 90°, whereas counterstreaming ME electron fluxes correspond to an electron boundary layer formed of previously accelerated magnetosheath electrons associated with a relative low-electron temperature (∼100 eV) and a higher parallel temperature than perpendicular. Note that the spacecraft potential is high (∼20 V, see black line in Figures 2m and in Figure 1b) in this region; therefore, although corrected, LE electron fluxes can be contaminated. At the end of this period, the increase of the ME electron fluxes around 180° generates a parallel current of ∼100 nA m^{-2}. Then ME and HE PAD spectrograms show that antiparallel HE electron fluxes sharply decrease after 1305:43.5 UT. This suggests the opening of the magnetic field lines northward of the MMS location, which would prevent HE electrons bouncing back from northward mirror points from reaching the satellites. This period of escaping electrons also corresponds to the period of intense electric and magnetic fluctuations and strong density gradient (see Figure 1). Therefore, in addition to LHDI, an electron beam instability could be responsible for the high-frequency part of the electric fluctuations [*Graham et al.*, 2016]. This short time period of escaping high-energy electrons corresponds to an antiparallel current ∼−200 nA m^{-2}. At the same time, the ion energy time spectrogram shows the presence of cold magnetosheath ions. More precisely, it seems that HE magnetospheric electrons, ME electrons (accelerated in the antiparallel direction), and entering cold ions are mixed between 1305:43.0 and 1305:43.5 UT. This region may correspond to the magnetospheric separatrix. Between 1305:45.0 and 1305:46.5 UT, on the magnetosheath side ($N_e \sim 10$ cm^{-3}), LE electron fluxes show a counterstreaming population. This population can be interpreted as a population trapped by a parallel electrostatic potential [*Egedal et al.*, 2008] which could develop along the newly reconnected field lines. Furthermore, for the present event we do not observe the pitch angle isotropization shown by *Lavraud et al.* [2016] because the estimated curvature radius of the magnetic field lines (not shown) is never smaller than 100 km while the Larmor radius for thermal electrons is about 1–3 km. Then a very short duration increase of LE electron fluxes in the antiparallel

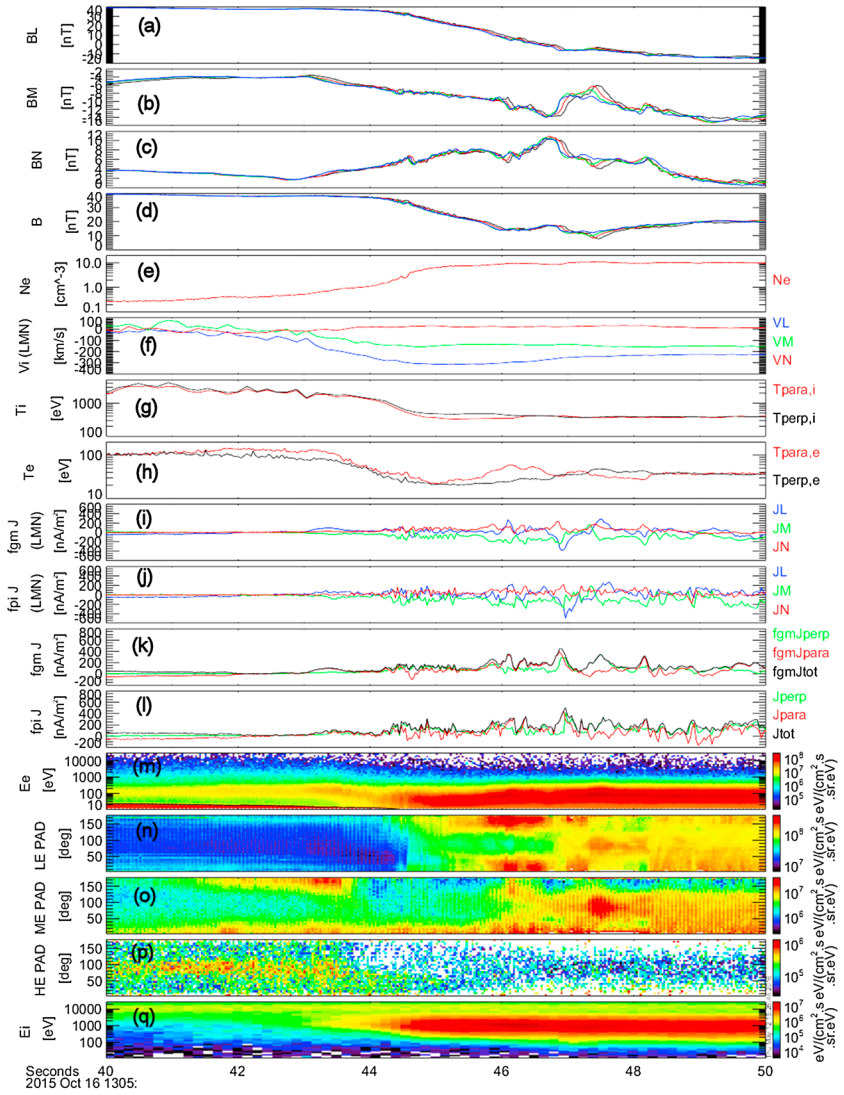

Figure 2. Between 1305:40 and 1305:50 UT in LMN coordinates: (a) BL,(b) BM, (c) BN, (d) B FGM data, (e) N_e, (f) V_i, (g) T_i, (h) T_e, (i) FGM current, (j) FPI current, (k) parallel, perpendicular, and total FGM currents, (l) same for FPI currents, (m) electron omnidirectional energy time spectrogram (with superposed spacecraft potential, black line), (n) low-energy (LE), (o) medium-energy (ME), and (p)high-energy (HE) pitch angle distribution (PAD) spectrograms, (q) ion omnidirectional energy time spectrogram.

direction produces a strong parallel current of up to 400 nA m^{-2} followed by a period from 1305:47.1 to 1305:48.1 UT of large perpendicular fluxes of LE and ME electrons corresponding to a strong perpendicular current of ~400 nA m^{-2} and a perpendicular temperature anisotropy. In the next section, we investigate how wave-particle interactions could be related to these different current and particle signatures.

3. Wave-Particle Interactions

Figure 3a shows again MMS1 FGM burst data in LMN coordinates as reference. Figures 3b and 3c present EDP and SCM waveforms which have been high-pass filtered above 32 Hz and projected into a magnetic field-aligned (MFA) coordinate system. This MFA frame is computed using a 30 ms averaged magnetic field. The *z* component corresponds to the magnetic field direction, the *y* direction is obtained from the cross product of the *z* vector and the GSE *x* direction, and the last one is the cross product of the first two. Omnidirectional E PSD and B PSD from 32 to 4096 Hz at 31 ms time resolution are plotted in Figures 3d and 3e. Figures 3f and 3g show the results of the wave polarization analysis obtained from the spectral matrix computed using SCM waveforms [*Samson and Olson*, 1980]: wave angle and ellipticity. From this analysis we

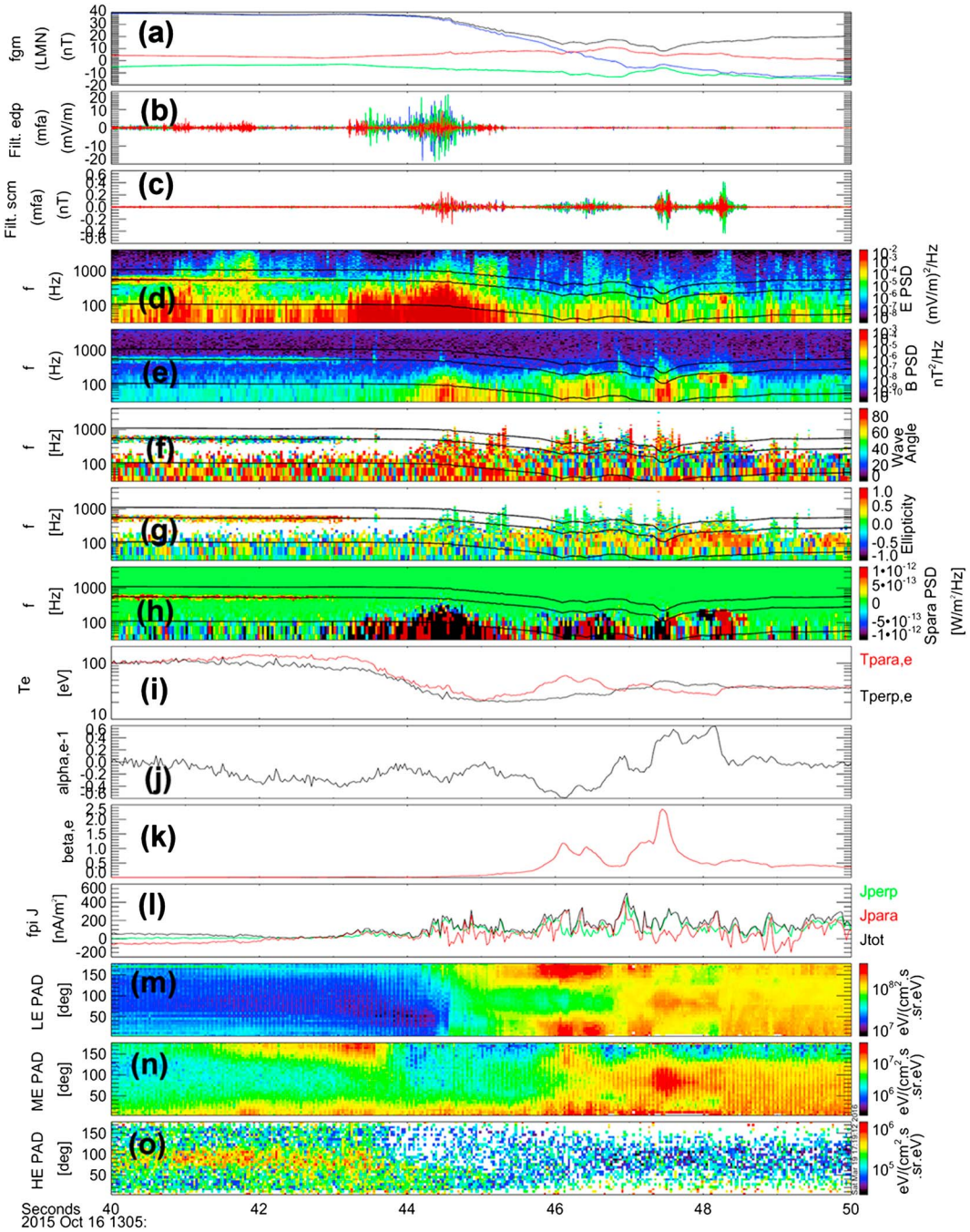

Figure 3. Between 1305:40 and 1305:50 UT, (a) **B** data in LMN, (b, c) high-pass filtered above 32 Hz EDP and SCM waveforms in magnetic field-aligned coordinate (MFA), (d, e) omnidirectional E and B PSD, (f) wave angle, (g) ellipticity, (h) parallel component of the Poynting vector, (i) T_e, (j) $\alpha - 1$ with $\alpha = T_{\perp,e}/T_{\|,e}$), (k) β_e the ratio between parallel electron thermal pressure and magnetic pressure, (l) FPI currents, (m) LE [0–200eV] PAD, (n) ME [200eV–2keV] PAD, (o) HE [2keV–30keV] PAD.

can identify the high-frequency emission detected on the magnetospheric side as whistler mode waves with $f \sim 0.5\ f_{ce} \sim 600$ Hz. Indeed, the corresponding ellipticity is close to +1, equivalent to a right-hand circular polarization. The associated wave angle is not always clearly estimated but varies from 0 to 40°. So the propagation can be quasi-parallel or oblique. This is confirmed by the fact that the parallel component of **E** can be as large as the perpendicular component of up to ~±2 mV/m. In the magnetosheath region, two groups of intense whistler emissions propagating in the quasi-parallel direction are detected between 0.1 and 0.5 f_{ce}, as

well as some less intense emissions above 0.5 f_{ce}. The first group occurs between 1305:46 and 1305:47 UT and the second more intense emissions between 1305:47 and 1305:48.500 UT. Panel Figure 3h shows the parallel component of the Poynting vector and indicates that the whistler mode wave emission on the magnetospheric side propagates northward (toward the reconnection region) in the direction parallel to the magnetic field (Spara > 0), suggesting that the source of this emission is located southward of the satellite. Although the amplitude of these waves is modulated, their polarization and direction of propagation are quasi-steady. *Vaivads et al.* [2007] showed that high-latitude *B* minima present on the dayside magnetosphere are a source of whistler waves and that the strongest emission occurs on the recently opened magnetospheric flux tubes. In our case, as explained previously, the opening of the magnetic field lines happens later and the whistler wave emissions occur on closed magnetic field lines. However, a high-latitude source in a *B* minima seems realistic, but needs to be confirmed by further studies. *Graham et al.* [2016] reported recently on a study based on Cluster data the same direction of propagation, but they found the whistler emissions being colocated with the magnetospheric separatrix region. Finally, for another magnetopause crossing event caught by MMS, *Wilder et al.* [2016] investigated the same type of whistler emissions and identified electrostatic solitary waves in phase with the parallel component of the whistler waves. In the magnetosheath region, the direction of propagation of the whistler mode waves is very fluctuating (alternatively toward and away from the reconnection region), suggesting that the source region could oscillate around the satellite location.

In a hot plasma, the electron temperature anisotropy $\alpha = T_{\perp,e}/T_{\|,e}$ is the source of the whistler anisotropy instability (WAI). A necessary condition for the growth of the WAI was given by *Kennel and Petschek* [1966] as: $\alpha - 1 > 1/(| f_{ce} | /f_r - 1)$, f_r being the real wave frequency. For $f_r \sim 0.3 f_{ce}$, it leads to $\alpha - 1 > 0.43$. Its maximum growth rate is obtained for strictly parallel or antiparallel propagation. Furthermore, *Gary and Wang* [1996] showed that for large $\beta_{\|,e}$ (defined as $N_e T_{\|,e}/P_B$ with P_B being the magnetic pressure) the anisotropy needed to make the WAI unstable is reduced. This was further confirmed by statistical analysis of Cluster data in the magnetosheath [*Gary et al.*, 2005] and numerical simulations [*Fujimoto and Sydora*, 2008]. Figures 3i–3k show the parallel and perpendicular electron temperatures, the term $\alpha - 1$ and $\beta_{\|,e}$, respectively. These parameters show that locally the conditions for the WAI growth are not fulfilled in the magnetosphere as there is no perpendicular temperature anisotropy and $\beta_{\|,e}$ is very small. However, the perpendicular anisotropy of HE electrons could be sufficient to generate these emissions or to sustain their propagation. Conversely, between 1305:47.5 and 1305:48.1 UT, the temperature anisotropy is strong ($\alpha - 1 > 0.4$) and $\beta_{\|,e}$ is close or larger than 1, consistent with a spacecraft location in the source region. The less intense emission between 1305:46 and 1305:47 UT does not correspond to a perpendicular temperature anisotropy although $\beta_{\|,e}$ is still close to 1. However, for this emission, perpendicular ME and HE electron fluxes are larger than parallel fluxes, which could explain that the medium- and high-energy parts of the electron distribution are locally unstable, although with smaller growth rate. Figures 4a and 4b show E and B PSD in magnetic field-aligned coordinates between 1305:35.0 and 1305:43.5 UT in the closed field line region and we recognize the strong whistler mode wave emission between 400 and 700 Hz (with $f \sim 0.5 f_{ce}$). The parallel E field component becomes as large as the perpendicular one, suggesting that on average, the oblique propagation is dominant. For such oblique propagations, whistler waves can accelerate electrons [e.g., *Mourenas et al.*, 2012]. The corresponding phase velocity (Figure 4c) is about 70,000 km s^{-1}. Except for the whistler mode wave emission, E and B spectra follow a power law, yet the level of B fluctuations are very close to the SCM noise floor (black line in Figures 4b). Also, above 100 Hz, the parallel E field component starts to be larger than the perpendicular component (Figures 4a and 4d), suggesting that a different wave mode is rising. As the level of the magnetic fluctuations is very low (close to the SCM noise floor), this wave mode is likely electrostatic. Figures 4e and 4f show the same plots between 1305:44 and 130546:10 UT in the magnetosheath. Again, the whistler mode wave emissions are identified in the B spectra around 200 Hz and 600 Hz, whereas the E components are much lower. The estimated phase velocities are between 6000 and 20,000 km s^{-1}. In this region, the parallel E field component starts to be larger than the perpendicular component only above 700 Hz and could be associated with nonlinear electrostatic structures. The estimated phase velocities are consistent with those recently found by *Graham et al.* [2016]. In the same manner, we calculate the parallel wavelengths and resonant velocities for magnetospheric (respectively, low-frequency magnetosheath) whistler mode wave emissions and find $\lambda_\| = v_{ph}/f \sim 7 \times 10^4/600 = 116$ km (respectively, $\lambda_\| = 6000/180 = 33$ km) and $v_{\|res} = (f - f_{ce})\lambda_\| = (600-1000) \times 116 = 4.64 \times 10^4$ km s^{-1} (respectively, $v_{\|res} = (200-500) \times 33 = 9900$ km s^{-1} which correspond to 6.1 keV (respectively 280 eV). Therefore, for the magnetospheric side with an electron temperature of about 100 eV and for the magnetosheath side with an average temperature of about 30 eV,

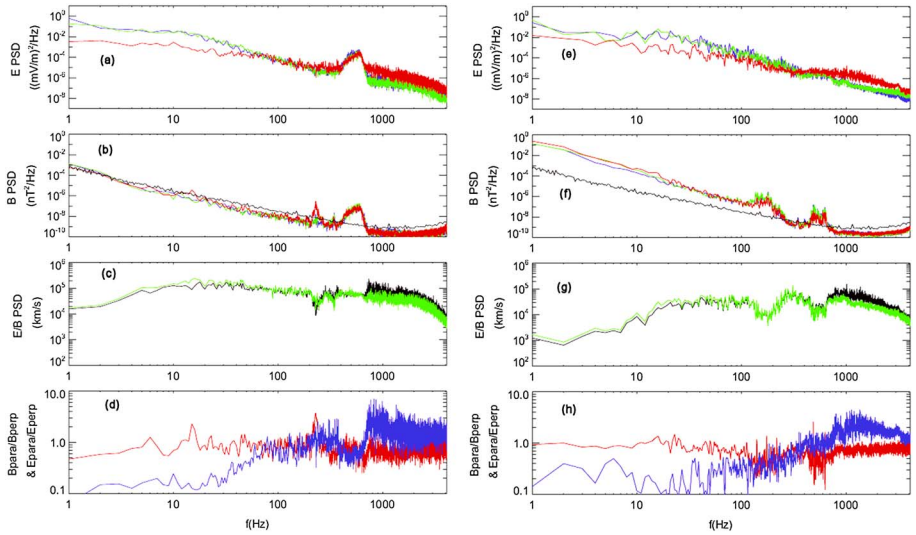

Figure 4. Between 1305:35 and 1305:43.5 UT corresponding to closed magnetic field line region: (a) E field power spectral densities (PSD) in MFA coordinates, (b) B PSD in MFA, (c) $|\mathbf{E}|/|\mathbf{B}|$ (black) and $|\mathbf{E}_\perp|/|\mathbf{B}_\perp|$ (green) which are estimates of wave phase velocity, (d) $B_\parallel/B_\perp$ (red)) PSD ratio and $E_\parallel/E_\perp$ (blue). Each spectrum corresponds to an average of eight spectra of 1 s time resolution. Figures 4e–4h have same legends for the period between 1305:44 and 1306:10 UT corresponding to the magnetosheath region. Each spectrum corresponds to an average of 25 spectra of 1 s time resolution.

the resonant electrons are always in the high-energy part of the distribution for which the perpendicular anisotropy is present. To summarize, it seems that WAI is the source of the whistler mode waves measured in the magnetosphere as well as in the magnetosheath. On the magnetosphere side, the whistler waves are propagating toward the reconnection region, while on the magnetosheath side both directions of propagations are found. These results about the source of the whistler waves on the magnetosheath side are consistent with those obtained by *Tang et al.* [2013] during a crossing of the electron diffusion region by a THEMIS satellite. However, they found that the whistler waves were propagating away from the reconnection region and suggested that the electron diffusion region could be the source region. Our results suggest that the magnetosheath separatrix region could be also a possible source region.

4. Ohm's Law

Although we need to be cautious when we use a fluid approach in a context where the spatial scales can be on the order of the ion or electron Larmor radii, to the first order we can estimate the different terms of the generalized Ohm's law which, in the absence of resistivity and neglecting the electron inertial term, can be written in the following form [e.g., *Vasyliunas*, 1975]:

$$\mathbf{E} = -\mathbf{V_i} \times \mathbf{B} + \frac{\mathbf{j} \times \mathbf{B}}{n_e q_e} - \frac{\nabla \cdot \mathbf{P_e}}{n_e q_e} \tag{1}$$

Here we will not estimate the electron pressure tensor term and just consider the electric field and the first two terms of the right-hand side. Figures 5f–5h show a comparison in LMN coordinates between **E** measured by EDP (blue), $-\mathbf{V_i} \times \mathbf{B}$ (black), $\mathbf{j}_{\mathrm{fgm}} \times \mathbf{B}/(n_e q_e)$ (green), and $-\mathbf{V_e} \times \mathbf{B}$ (red). Ions are decoupled from the magnetic field line motion due to the Hall effect (~5 mV m^{-1}) between 1305:42 and 1306:46 UT (a region having a spatial scale of few ion inertial lengths or few Larmor radii) while electrons are still moving with **B**. It also corresponds to the period of the opening of the magnetic field lines, the escaping of high-energy magnetospheric electrons ($j_\parallel \sim -200$ nA m^{-2} and $j_\perp \sim 200$ nA m^{-2}) and the entry of cold magnetosheath ions (see Figure 2). This region has been identified previously as the magnetospheric separatrix region and analyzed in detail [e.g., *Mozer et al.*, 2002; *Khotyaintsev et al.*, 2006; *Retinò et al.*, 2006]. Figures 5o–5q show that the Hall effect is also present on the magnetosheath side but with smaller amplitude due to a larger density. In particular, the perpendicular current peak at 1305:46.9 UT corresponds to a Hall electric field along the normal EN ~2 mV m^{-1} which decouples ions from electrons and magnetic field lines. The comparison for the EL component

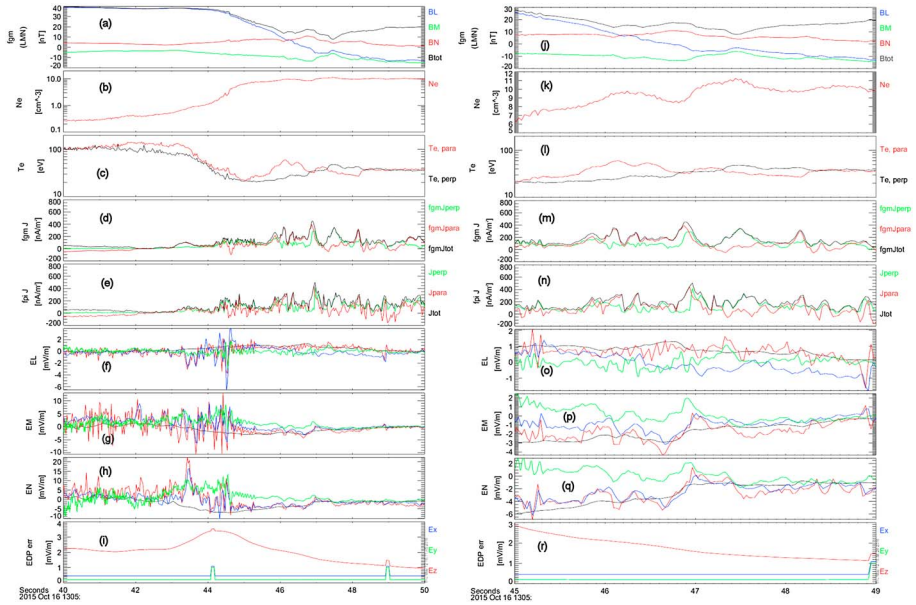

Figure 5. Between 1305:40 and 1305:50 UT: (a) **B** data, (b) N_e, (c) T_e, (d) parallel, perpendicular, and total FGM and (e) FPI currents, (f, g, h) comparison between EDP E field data (blue), $-\mathbf{V}_e \times \mathbf{B}$ (red), $-\mathbf{V}_i \times \mathbf{B}$ (black) and $\mathbf{j}_{\mathrm{fgm}} \times \mathbf{B}/(n_e q_e)$ (green, the Hall field), (i) error on each electric field component (in sensor frame). In the magnetospheric region, BL is mainly along Z GSE which is almost in the direction of the axial double probes, so the error on Ez is mainly reported on EL. (j–r) Same legends for the time period between 1305:45 to 1305:49 UT in the magnetosheath region.

(Figure 5o) between 1305:46.4 and 1305:48.8 shows a discrepancy of ~1–2 mV m^{-1} with $\mathbf{V_i} \times \mathbf{B}$, $\mathbf{V_e} \times \mathbf{B}$ and $\mathbf{E}$ which is likely due to the fact that as BL goes to zero, the perpendicular electric field component is also measured by the axial double probes which have a larger error bar, as shown in Figure 5r. Around 1305:47 UT, EN changes sign after the strong perpendicular current ($j_\perp \sim$ 400 nA m^{-2}) associated with the intense whistler wave emission and as BL becomes negative suggesting that MMS is now located close to the magnetosheath separatrix region [*Pritchett*, 2008].

5. Summary and Conclusion

We have reported MMS observations which show that quasi-steady magnetospheric whistler mode wave emissions at $f \sim f_{ce}/2$ propagating toward the reconnection region (northward) with quasi-parallel and oblique angles are detected just before MMS crosses the magnetopause and a southward ion flow. These whistler waves are likely generated by the perpendicular anisotropy of energetic magnetospheric electrons (WAI). The source of these whistler waves could be located at high-latitude B minima as shown by *Vaivads et al.* [2007]. Just after this emission ends, we identify the opening of the magnetic field lines when HE parallel electrons vanish and parallel and perpendicular currents are measured ($j_\parallel \sim -200$ nA m^{-2}, $j_\perp \sim 200$ nA m^{-2}), consistent with a magnetospheric separatrix region. In this region, the calculated Hall field is consistent with the decoupling of ions from the magnetic field. Then counterstreaming LE electron fluxes are detected on the magnetosheath side, possibly trapped by a parallel electrostatic potential [*Egedal et al.*, 2008] Finally, large parallel and perpendicular current signatures and intense quasi-parallel whistler mode wave emissions propagating toward and away from the reconnection region are measured associated with a region of smaller Hall electric fields still consistent with the decoupling of the ions and with a magnetosheath separatrix region. Thus, the electron diffusion region [*Tang et al.*, 2013] as well as the magnetosheath separatrix could constitute different source regions of the whistler waves.

Acknowledgments
The French involvement (SCM) on MMS is supported by CNES and CNRS. H. B.'s work has been supported by CNES through grant "Allocations de recherche post-doctorale". O. Le Contel thanks the SPEDAS team and, in particular, V. Angelopoulos and E. Grimes for their efforts to include MMS data in SPEDAS. All MMS data used are available at https://lasp.colorado.edu/mms/sdc/public/about/browse-wrapper/

References

Birn, J., et al. (2001), Geospace Environmental Modeling (GEM) magnetic reconnection challenge, *J. Geophys. Res.*, *106*, 3715–3719.
Burch, J. L., T. E. Moore, R. B. Torbert, and B. L. Giles (2015), Magnetospheric multiscale overview and science objectives, *Space Sci. Rev.*, *199*, 5–21, doi:10.1007/s11214-015-0164-9.
Burch, J. L., et al. (2016), Electron-scale measurements of magnetic reconnection in space, *Science*, doi:10.1126/science.aaf2939.
Cattell, C., J. Wygant, F. S. Mozer, T. Okada, K. Tsuruda, S. Kokubun, and T. Yamamoto (1995), ISEE 1 and Geotail observations of low-frequency waves at the magnetopause, *J. Geophys. Res.*, *100*, 11,823–11,829, doi:10.1029/94JA03146.

Chanteur, G., and C. Harvey (1998), Spatial interpolation for four spacecraft: Application to magnetic gradients, in *Analysis Methods for Multi-Spacecraft Data, ISSI Sci. Rep. SR-001*, edited by G. Paschman and P. Daly, chap. 15, pp. 371–393, Eur. Space Agency, Berlin.

Chaston, C., J. Bonnell, J. P. McFadden, C. W. Carlson, C. Cully, O. Le Contel, A. Roux, H. U. Auster, K. H. Glassmeier, V. Angelopoulos, and C. T. Russell (2008), Turbulent heating and cross-field transport near the magnetopause from THEMIS, *Geophys. Res. Lett.*, *35*, L17S08, doi:10.1029/2008GL033601.

Deng, X. H., and H. Matsumoto (2001), Rapid magnetic reconnection in the Earth's magnetosphere mediated by whistler waves, *Nature*, *410*, 557–560.

Egedal, J., W. Fox, N. Katz, M. Porkolab, M. Øieroset, R. P. Lin, W. Daughton, and J. F. Drake (2008), Evidence and theory for trapped electrons in guide field magnetotail reconnection, *J. Geophys. Res.*, *113*, A12207, doi:10.1029/2008JA013520.

Ergun, R. E., et al. (2014), The axial double probe and fields signal processing for the MMS mission, *Space Sci. Rev.*, *199*, 167–188, doi:10.1007/s11214-014-0115-x.

Fujimoto, K., and R. D. Sydora (2008), Whistler waves associated with magnetic reconnection, *Geophys. Res. Lett.*, *35*, L19112, doi:10.1029/2008GL035201.

Gary, S. P., and J. Wang (1996), Whistler instability: Electron anisotropy upper bound, *J. Geophys. Res.*, *101*, 10,749–10,754.

Gary, S. P., B. Lavraud, M. F. Thomsen, B. Lefebvre, and S. J. Schwartz (2005), Electron anisotropy constraint in the magnetosheath: Cluster observations,*Geophys. Res. Lett.*, *32*, L13109, doi:10.1029/2005GL023234.

Graham, D. B., A. Vaivads, Y. V. Khotyaintsev, and M. André (2016), Whistler emission in the separatrix regions of asymmetric magnetic reconnection, *J. Geophys. Res. Space Physics*, *121*, 1934–1954, doi:10.1002/2015JA021239.

Kennel, C. F., and H. E. Petschek (1966), Limit on stably trapped particle fluxes, *J. Geophys. Res.*, *71*, 1–28.

Khotyaintsev, Y. V., A. Vaivads, A. Retinò, M. André, C. J. Owen, and H. Nilsson (2006), Formation of inner structure of a reconnection separatrix region, *Phys. Rev. Lett.*, *97*(20), 205003, doi:10.1103/PhysRevLett.97.205003.

Lavraud, B., et al. (2016), Currents and associated electron scattering and bouncing near the diffusion region at Earth's magnetopause, *Geophys. Res. Lett.*, *43*, 3042–3050, doi:10.1002/2016GL068359.

Le Contel, O., R. Pellat, and A. Roux (2000), Self-consistent quasi-static radial transport during the substorm growth phase, *J. Geophys. Res.*, *105*, 12,929–12,944.

Le Contel, O., et al. (2014), The search-coil magnetometer for MMS, *Space Sci. Rev.*, *199*, 257–282, doi:10.1007/s11214-014-0096-9.

Lindqvist, P.-A., et al. (2014), The spin-plane double probe electric field instrument for MMS, *Space Sci. Rev.*, *199*, 137–165, doi:10.1007/s11214-014-0116-9.

Mourenas, D., A. Artemyev, O. Agapitov, and V. Krasnoselskikh (2012), Acceleration of radiation belts electrons by oblique chorus waves, *J. Geophys. Res.*, *117*, A10212, doi:10.1029/2012JA018041.

Mozer, F. S., S. D. Bale, and T. D. Phan (2002), Evidence of diffusion regions at a subsolar magnetopause crossing, *Phys. Rev. Lett.*, *89*(1), 015002, doi:10.1103/PhysRevLett.89.015002.

Mozer, F. S., P. L. Pritchett, J. Bonnell, D. Sundkvist, and M. T. Chang (2008), Observations and simulations of asymmetric magnetic field reconnection, *J. Geophys. Res.*, *113*, A00C03, doi:10.1029/2008JA013535.

Paschmann, G., I. Papamastorakis, W. Baumjohann, N. Sckopke, C. Carlson, B. Ö. Sonnerup, and H. Lühr (1986), The magnetopause for large magnetic shear: AMPTE/IRM observations, *J. Geophys. Res.*, *91*, 11,099–11,115.

Pritchett, P. L. (2008), Collisionless magnetic reconnection in an asymmetric current sheet, *J. Geophys. Res.*, *113*, A06210, doi:10.1029/2007JA012930.

Pritchett, P. L., and F. S. Mozer (2009), The magnetic field reconnection site and dissipation region, *Phys. Plasmas*, *16*(8), 080702, doi:10.1063/1.3206947.

Retinò, A., et al. (2006), Structure of the separatrix region close to a magnetic reconnection X-line: Cluster observations, *Geophys. Res. Lett.*, *33*, L06101, doi:10.1029/2005GL024650.

Roux, A., P. Robert, O. Le Contel, V. Angelopoulos, U. Auster, J. Bonnell, C. M. Cully, R. E. Ergun, and J. P. McFadden (2011), A mechanism for heating electrons in the magnetopause current layer and adjacent regions, *Ann. Geophys.*, *29*, 2305–2316, doi:10.5194/angeo-29-2305-2011.

Russell, C. T., et al. (2014), The magnetospheric multiscale magnetometers, *Space Sci. Rev.*, *199*, 189–256, doi:10.1007/s11214-014-0057-3.

Samson, J. C., and J. V. Olson (1980), Some comments on the descriptions of the polarization states of waves, *Geophys. J. R. Astron. Soc.*, *61*, 115–129.

Scudder, J. D., R. D. Holdaway, R. Glassberg, and S. L. Rodriguez (2008), Electron diffusion region and thermal demagnetization, *J. Geophys. Res.*, *113*, A10208, doi:10.1029/2008JA013361.

Shue, J.-H., et al. (1998), Magnetopause location under extreme solar wind conditions, *J. Geophys. Res.*, *103*, 17,691–17,700, doi:10.1029/98JA01103.

Sonnerup, B. Ö., I. Papamastorakis, G. Paschmann, and H. Lühr (1987), Magnetopause properties from AMPTE/IRM observations of the convection electric field: Method development, *J. Geophys. Res.*, *92*, 12,137–12,159.

Swisdak, M., B. N. Rogers, J. F. Drake, and M. A. Shay (2003), Diamagnetic suppression of component magnetic reconnection at the magnetopause, *J. Geophys. Res.*, *108*(A5), 1218, doi:10.1029/2002JA009726.

Tang, X., C. Cattell, J. Dombeck, L. Dai, L. B. Wilson, A. Breneman, and A. Hupach (2013), THEMIS observations of the magnetopause electron diffusion region: Large amplitude waves and heated electrons, *Geophys. Res. Lett.*, *40*, 2884–2890, doi:10.1002/grl.50565.

Torbert, R. B., et al. (2014), The FIELDS instrument suite on MMS: Scientific objectives, measurements, and data products, *Space Sci. Rev.*, *199*, 105–135, doi:10.1007/s11214-014-0109-8.

Treumann, R. A. (2001), Origin of resistivity in reconnection, *Earth Planets Space*, *53*, 453–462, doi:10.1186/BF03353256.

Vaivads, A., M. André, S. C. Buchert, J.-E. Wahlund, A. N. Fazakerley, and N. Cornilleau-Wehrlin (2004), Cluster observations of lower hybrid turbulence within thin layers at the magnetopause, *Geophys. Rev. Lett.*, *31*, L03804, doi:10.1029/2003GL018142.

Vaivads, A., O. Santolík, G. Stenberg, M. André, C. J. Owen, P. Canu, and M. Dunlop (2007), Source of whistler emissions at the dayside magnetopause, *Geophys. Res. Lett.*, *34*, L09106, doi:10.1029/2006GL029195.

Vasyliunas, V. M. (1975), Theoretical models of magnetic field line merging. I, *Rev. Geophys. Space Phys.*, *13*, 303–336, doi:10.1029/RG013i001p00303.

Wilder, F. D., et al. (2016), Observations of Whistler-mode Waves with Non-linear Parallel Electric Fields near the Dayside Magnetic Reconnection Separatrix by the Magnetospheric Multiscale Mission, *Geophys. Res. Lett.*, doi:10.1002/2016GL069473.

Wygant, J. R., et al. (2005), Cluster observations of an intense normal component of the electric field at a thin reconnecting current sheet in the tail and its role in the shock-like acceleration of the ion fluid into the separatrix region, *J. Geophys. Res.*, *110*, A09206, doi:10.1029/2004JA010708.

Erratum

In the originally published version of this article, figure 5 was incorrectly typeset. The figure conversion error has since been corrected, and this version may be considered the authoritative version of record.